Statistical investigation of the effect of Coulomb collisions on thermodynamic evolution of the Alfvénic slow wind

Jimin Hong[1], Jungjoon Seough[2,3], Kyungguk Min[1]

Abstract

Coulomb collisions are believed to be one of the physical mechanisms leading to thermodynamic equilibrium of solar wind plasma. In this study, we investigate the effect of Coulomb collisions on the thermodynamic evolution of protons in the Alfvénic slow wind by analyzing the Helios data during the solar minimum of solar cycle 21 (1975-1977). We classify the Alfvénic slow wind into three groups according to the proton specific entropy. For each group, called a stream, we analyze the radial evolution of the macroscopic quantities (proton density, temperature, etc.) of the proton species to diagnose the thermodynamic evolution of the Alfvénic slow wind associated with that stream. We find that Coulomb collisions could play a role in regulating the proton temperature anisotropy in the stream associated with the lowest entropy, leading to thermal equilibrium of the proton species at 1 au. We suggest that the three different Alfvénic slow streams categorized by the value of proton specific entropy might originate from different solar source regions.

1. Introduction

The solar wind is a supersonic and super-Alfvénic flow of plasma emanating from the Sun and traveling through interplanetary space. Since a plasma is a group of charge particles, its dynamics are governed by the electric and magnetic fields that permeate through the plasma. In a dense neutral gas, collisions between particles occur frequently, which are common binary collisions. Collisions also occur in space plasmas, but their nature is different: Since the density is low and particles (mainly electrons and protons) are charged, collisions in the plasma are mediated dominantly by the Coulomb force (Dougal & Goldstein 1958; Meyer-Vernet 2007), in which case they are called Coulomb collisions.

[1] Department of Astronomy and Space Science, Chungnam National University, Daejeon, Republic of Korea
[2] Korea Astronomy and Space Science Institute, Daejeon, Republic of Korea
[3] seough@kasi.re.kr

Initially, the solar wind plasma was considered as being weakly collisional because of its low number density and high temperature (e.g., Barnes 1968; Chen et al. 1972). According to the adiabatic Chew-Goldberger-Low (CGL) relationship (Chew et al. 1956), the solar wind plasma evolves with a radial distance (R) from the Sun so that the temperature parallel to the background magnetic field ($\mathbf{B_0}$) remains constant ($T_{\parallel} \propto const$) and the temperature perpendicular to $\mathbf{B}_0$ varies as $T_{\perp} \propto R^{-2}$. The in-situ measurements, however, showed that the solar wind does not follow the simple CGL relationship (e.g., Matteini et al. 2007; Hellinger et al. 2011; Huang et al. 2020). Heating through Alfvén waves and turbulences mainly affects $T_{\perp}$ so that it decreases more slowly than the R^{-2} dependence of the CGL relation. As a result, such heating can destroy the ideal plasma double-adiabatic invariants (Chandran et al. 2010; van Ballegooijen & Asgari-Targhi 2016; Perez et al. 2021). In addition, $T_{\parallel}$ no longer remains constant but decreases with R, when the spiral geometry of the interplanetary magnetic field is taken into account (Hellinger et al. 2011; Perrone et al. 2019). More recently, Coulomb collisions are believed to be important on the thermodynamic evolution of the solar wind plasma. Coulomb collisions cause slow loss of energy in the electron strahl, break the plasma double-adiabatic invariants, and change the ion velocity distribution (Marsch & Goldstein 1983; Hellinger & Trávníček 2014; Boldyrev et al. 2020; Huang et al. 2020). In particular, Coulomb collisions change the temperature anisotropy of electrons and ions, causing the solar wind to quickly reach thermal equilibrium (e.g., Klein et al. 1985; Salem et al. 2003; Kasper et al. 2008; Štverák et al. 2008; Bale et al. 2009; Yoon et al. 2019). Bale et al. (2009) suggested that an isotropic plasma can be caused by Coulomb collisions. Still to date, it is not well understood as to how the various processes mentioned above operate to affect the solar wind plasma evolution. A particular emphasis of the present study is to understand the effect of Coulomb collisions on the thermodynamic evolution of the slow solar wind.

It is known that the thermodynamic evolution of the solar wind depends on the characteristics of the solar wind. The fast (solar) wind generally has a speed more than $600\ km/s$ and is believed to originate in the polar coronal holes. The slow (solar) wind, with speed at less than $400 - 500\ km/s$, is believed to have its origin in the streamer structures or the active regions (Meyer-Vernet 2007; Abbo et al. 2016; Stansby 2019). The fast wind usually exhibits higher Alfvénicity, which means that the plasma has the characteristic of Alfvén waves. In contrast, the slow wind has lower Alfvénicity (i.e., no Alfvén waves). Nevertheless, recent studies show that some slow winds can have a high Alfvénicity, in which case these are called the Alfvénic slow wind distinguishing it from the typical, non-Alfvénic slow wind. Although the Alfvénic slow wind has the characteristics of Alfvén waves, unlike fast wind, it has a relatively slow speed and is not collision-less (D'Amicis et al. 2019; Stansby et al. 2019; Wang et al. 2019; Wang & Ko 2019; Perrone et al. 2020). The thermodynamic properties of the Alfvénic slow wind seem to be different from those of the fast and non-Alfvénic slow winds. For example, Huang et al. (2020) shows that the Alfvénic slow wind reaches thermodynamic equilibrium faster than the fast wind. The recent classification of Alfvénic slow winds and their distinct radial evolution motivate us to further investigate the thermodynamic properties of the Alfvénic slow wind.

In this paper, we classify the solar wind into three types using the solar wind speed and Alfvénicity, and statistically investigate the effect of Coulomb collisions in each type. The fast wind is clearly collision-less, whereas it is expected that collisions occur quite frequently in the slow wind. As a result, we expect that the radial evolution of the proton temperature anisotropy will be different depending on the types of solar wind classified. We can consider that the plasma reaches thermodynamic equilibrium, when the proton distribution becomes isotropic. Coulomb collisions are believed to affect this process. In order to investigate this effect, we select unperturbed plasma intervals of Alfvénic slow wind and analyze its radial evolution. In addition, we discuss possible source regions of Alfvénic slow wind using the proton specific entropy, which appears to track the heavy ion ratio (specifically for carbon and oxygen ions) of the solar wind.

2. Data Analysis

2.1. Helios Mission & Data Used

The Helios mission consists of twin spacecraft launched in 1974 and 1976, respectively. They were located close to the ecliptic plane with an orbital inclination of 0.02º, and carried out inner heliosphere observation missions (Porsche 1977). Prior to the launch of Parker Solar Probe in 2018 (Fox et al. 2016), they were the closest spacecraft to the Sun. The orbits of the twin spacecraft covered the interplanetary space from Mercury to Earth orbits, with perihelion approximately at 0.3 au and aphelion at 1 au. The spacecraft were equipped with an E1 plasma instrument to detect solar wind plasma, which measures and provides the distribution function and moment of electrons and ions (Schwenn et al. 1975), and fluxgate magnetometers (E2 and E3) for magnetic field measurement (Musmann et al. 1975; Scearce et al. 1975).

Recently, Stansby et al. (2018) re-processed the original Helios ion distribution functions to provide reliable and reproducible data to characterize the proton core population of the solar wind in the inner heliosphere. Performing a systematic fitting of bi-Maxwellian distribution functions to the raw Helios ion data, they tabulated the proton core number density, velocity, and temperatures parallel and perpendicular to the magnetic field; this processed dataset is called the core-fit data. These parameters for the proton core population are provided in the RTN coordinate system with an average interval of 40.5 seconds and used in this study to investigate the thermodynamic evolution of the slow Alfvénic solar wind.

2.2. Method

To identify Alfvénic slow winds among the slow wind data, Alfvénicity was calculated using the solar wind velocity and magnetic field data at 30-minute intervals. The Alfvénicity is defined as (Bruno & Carbone 2013; Wang et al. 2019)

$$\sigma_c = 2\frac{\langle \delta V \cdot \delta V_A \rangle}{\langle \delta V^2 + \delta V_A^2 \rangle}, \quad (1)$$

where $\delta V = V - \langle V \rangle$ denotes the deviation of the proton velocity from the 30-minute average and $\delta V_A = (B - \langle B \rangle) / \sqrt{\mu_0 \langle \rho \rangle}$ similarly denotes the deviation of the magnetic field from the mean value. Here, μ_0 is the magnetic permeability in vacuum, ρ is the proton mass density, and $\langle \cdots \rangle$ indicates a 30-minute average of the associated quantity. The value $|\sigma_c| \simeq 1$ means that the solar wind plasma has the characteristic of Alfvén waves, and $|\sigma_c| < 1$ means non-Alfvénic solar wind (Perrone et al. 2020). The sign of σ_c indicates the propagation direction of Alfvén waves with respect to the background magnetic field; only the magnitude of σ_c is used for the present analysis. To reduce the human bias, the identification of Alfvénic slow wind is aided by an un-supervised machine learning technique, called the TimeSeriesKMeans algorithm (Sakoe & Chiba 1978; Cuturi & Blondel 2017). This algorithm calculates the similarity between time series and then automatically clusters them. The detailed description of this algorithm can be found in the Tslearn library documentation[4]. In this study, the solar wind with Alfvénicity $|\sigma_c| \geq 0.7$ is considered as a Alfvénic solar wind; the same criterion was used previously by Wang et al. (2019).

Proton total temperature and temperature anisotropy are defined as $T_p = (2T_\perp + T_\parallel) / 3$ and $T_\perp / T_\parallel$, respectively (Stansby et al. 2019). The ratio $T_\perp / T_\parallel \simeq 1$ means that solar wind plasma is close to thermodynamic equilibrium.

To investigate Coulomb collisions, we used the collisional frequency, which is defined as

$$\nu_{pp} = \sqrt{\frac{\pi}{m_p}} \times \frac{4ne^4 \ln \Lambda}{3\left(k_B T_p\right)^{3/2}}, \quad (2)$$

where m_p, n, e and k_B indicate the proton mass, number density, elementary charge, and the Boltzmann constant, respectively; $ln\,\Lambda$ is the Coulomb logarithm; and $\Lambda = 3\left(k_B T_p\right)^{3/2} / 2e^3\sqrt{n\pi}$ (Schunk 1975; Chandran et al. 2011; Wilson et al. 2018). In this study, a collisional age is defined using ν_{pp} (e.g., Kasper et al. 2008; Bale et al. 2009; Chhiber et al. 2016; Kasper et al. 2017; D'Amicis et al. 2019; Verscharen et al. 2019).

$$A_c = \frac{R}{V_{sw}} \times \nu_{pp}^m, \quad (3)$$

where V_{sw} is the solar wind speed and R is the radial distance from the Sun. The collisional age of equation (3) is interpreted as the number of collisions a particle would have experienced to the point where the solar wind is observed. For example, $A_c = 1$ indicates that the solar wind plasma has undergone about one Coulomb collision until the observation point. A higher number means that the

[4] https://tslearn.readthedocs.io/

plasma is expected to experience many collisions, and vice versa. D'Amicis et al. (2019) suggested that the relatively lower A_c solar wind plasma can better preserve the processes that occur in the inner corona. In general, fast wind is expected to have lower collisional age due to low collisional frequency, resulting from low density and high temperature, whereas slow wind exhibits relatively higher collisional age.

Figure 1 shows a typical example of three-different types of solar winds obtained from the core-fit data of Helios 1. The solar wind denoted by the green box can be identified as a non-Alfvénic slow wind because of the isotropic temperature (Figure 1d), high collisional age (greater than 1; Figure 1e), and low Alfvénicity (Figure 1f). Although similar in characteristics with the first period, the period denoted by the red box may contain the Alfvénic slow wind exhibiting higher Alfvénicity (Figure 1f). These Alfvénic fluctuations may lead to the velocity spike (Figure 1a) similar to in situ measurements of solar wind speed obtained from the WIND spacecraft at 1 au (shown in the top panel of Figure 1 of D'Amicis et al. 2019). The typical characteristics of the fast wind are seen in the cyan box. That is, in this period the solar wind exhibits a large speed (over $600\ km/s$), low density ($\sim 10\ cm^{-3}$), large temperature anisotropy, low collisional age, and large Alfvénicity. In Figure 1f, the red and blue shadings denote the Alfvénic slow wind and non-Alfvénic slow wind, respectively, determined by the TimeSeriesKMeans algorithm. The fast wind and Alfvénic slow wind show similar Alfvénicity, whereas the non-Alfvénic slow wind is characterized by the wide range of Alfvénicity.

We analyzed the solar wind proton data by classifying it into three types during the Helios mission (1975-1985): fast wind with $V_{sw} \geq 600km/s$, Alfvénic slow wind with $V_{sw} \leq 450km/s$ and $|\sigma_c| \geq 0.7$, and non-Alfvénic slow wind with $V_{sw} \leq 450km/s$ and $|\sigma_c| < 0.7$. For these three types, Figure 2 shows the two-dimensional histograms in the $A_c - T_\perp / T_\parallel$ domain. In Figure 2a, the fast wind exhibits lower collisional age of about 0.01 and higher temperature anisotropy. It is interpreted as a fast wind evolving into a collision-less state in the inner heliosphere, which is consistent with the previous study (e.g., Barnes 1968; Chen et al, 1972; Marsch & Goldstein 1983; Livi et al. 1986). According to Perrone et al. (2019), high temperature anisotropy appears even near 1 au, which is thought to be associated with the perpendicular heating process, for example, Alfvén-wave turbulence (Chandran et al. 2011). Conversely, in Figure 2c, the non-Alfvénic slow wind is characterized by the large collisional age, and most of the events are observed to have isotropic temperature. It is interesting to note that Alfvénic slow wind is characterized by slow solar wind speed but has Alfvén waves similar to the fast wind. Consequently, the histogram in Figure 2b exhibits the characteristics of both types of solar wind. The Alfvénic slow wind tends to have relatively larger anisotropy in the smaller collisional age domain but has nearly isotropic temperature when the collisional age is greater than about 0.3, resulting from the effect of Coulomb collisions.

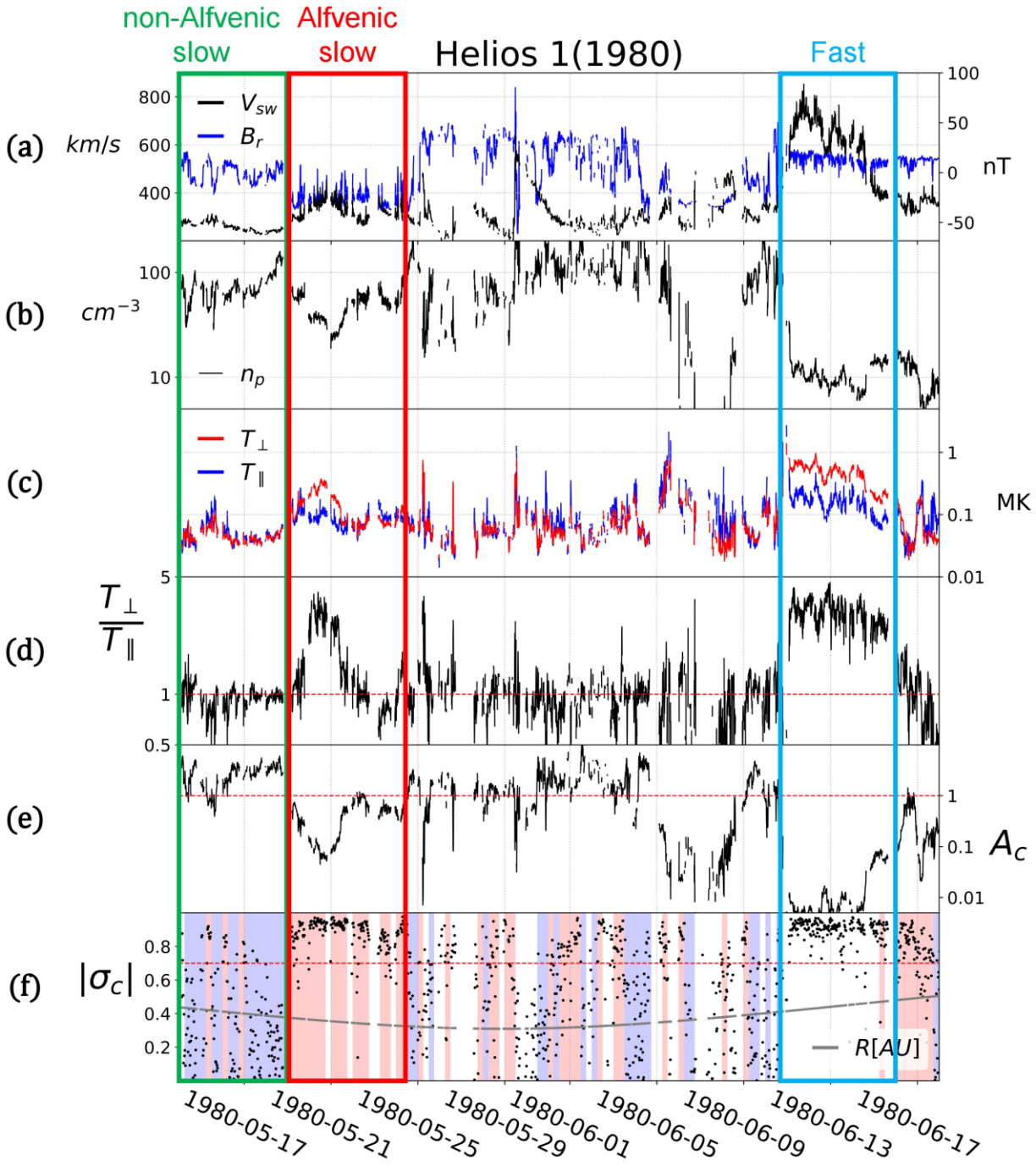

Figure 1. Helios-1 solar wind core-fit data in May to June 1980. (a) Solar wind speed (black) and magnetic field intensity (blue); (b) proton density; (c) proton temperatures, $\boldsymbol{T}_\perp$ (red) and $\boldsymbol{T}_\parallel$ (blue); (d) temperature anisotropy, $\boldsymbol{T}_\perp$ / $\boldsymbol{T}_\parallel$; (e) collisional age; and (f) Alfvénicity (black-dot). The red horizontal lines in (d-f) are drawn at $\boldsymbol{T}_\perp$ / $\boldsymbol{T}_\parallel = \mathbf{1}$, $\boldsymbol{A_c} = \mathbf{1}$, and $|\boldsymbol{\sigma_c}| = \mathbf{1}$, respectively. The gray curve in (f) denotes the radial distance of the spacecraft in au. The red and blue shadings in (f) indicate the Alfvénic slow wind and non-Alfvénic slow wind, respectively, identified by the TimeSeriesKMeans algorithm.

3. Results

3.1. Statistical analysis of the three-different types of solar wind

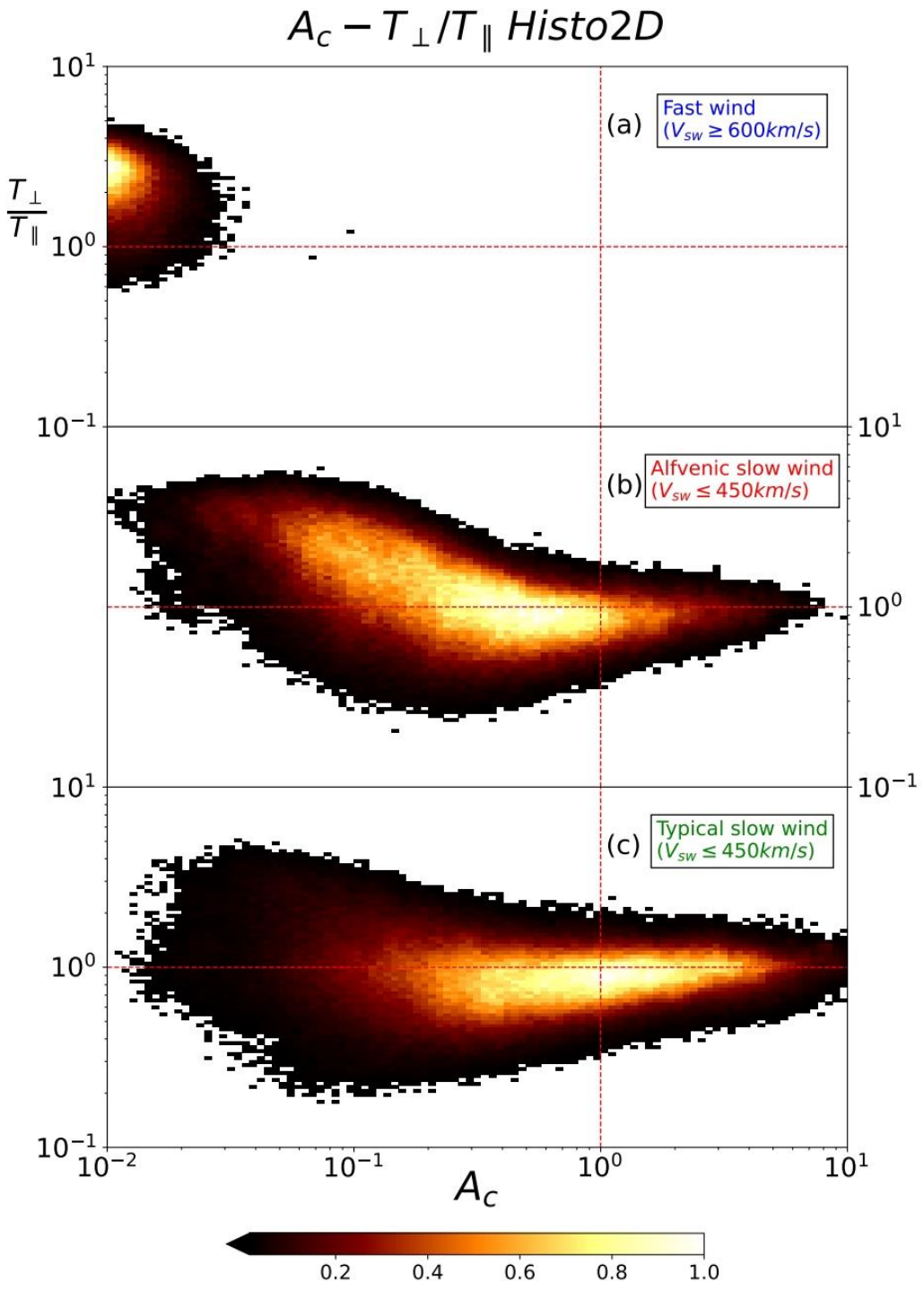

Figure 2. Two-dimensional histograms of the collisional age and temperature anisotropy for (a) fast, (b) Alfvénic slow, and (c) non-Alfvénic slow winds. Each histogram is normalized by the max count number for the corresponding solar wind type. The vertical and horizonal dashed lines are drawn at $\boldsymbol{A_c = 1}$ and $\boldsymbol{T_\perp / T_\parallel = 1}$, respectively.

Figure 3 shows the distribution of proton temperature anisotropy versus parallel plasma beta at the three different radial distances. The fast wind exhibits higher anisotropy regardless of the distance after being expanded into interplanetary space until reaching 1 au. This might be related to the perpendicular heating by Alfvén-wave turbulence, which occurs continuously through the interplanetary medium. The Alfvénic slow wind plasma is found to be anisotropic at radial distances below 0.4 au, which is relatively close to the sun, and events with higher Alfvénicity are generally observed. On the other hand, at radial distances beyond 0.9 au, the plasmas of both slow winds are found to be isotropic, and the number of Alfvénic slow wind events is also observed to be less than the number at radial distances below 0.4 au. This is because the Alfvénic slow wind plasma is heated by Alfvén waves, similar to the fast wind, and at the same time, experiences Coulomb collisions that isotropies the plasma.

To summarize, we have in this subsection distinguished three types of solar winds based on solar wind speed and Alfvénicity, and analyzed the effect of Coulomb collisions. The fast wind is clearly collision-less and the non-Alfvénic slow wind has proven to be collision-dominant. The Alfvénic slow wind is more collisional compared to the fast wind. In addition, the Alfvénic slow wind is anisotropic in a weakly collisional domain and isotropic in a collision-dominant domain. In the following subsection, we analyze in detail the thermodynamic evolution of the Alfvénic slow wind.

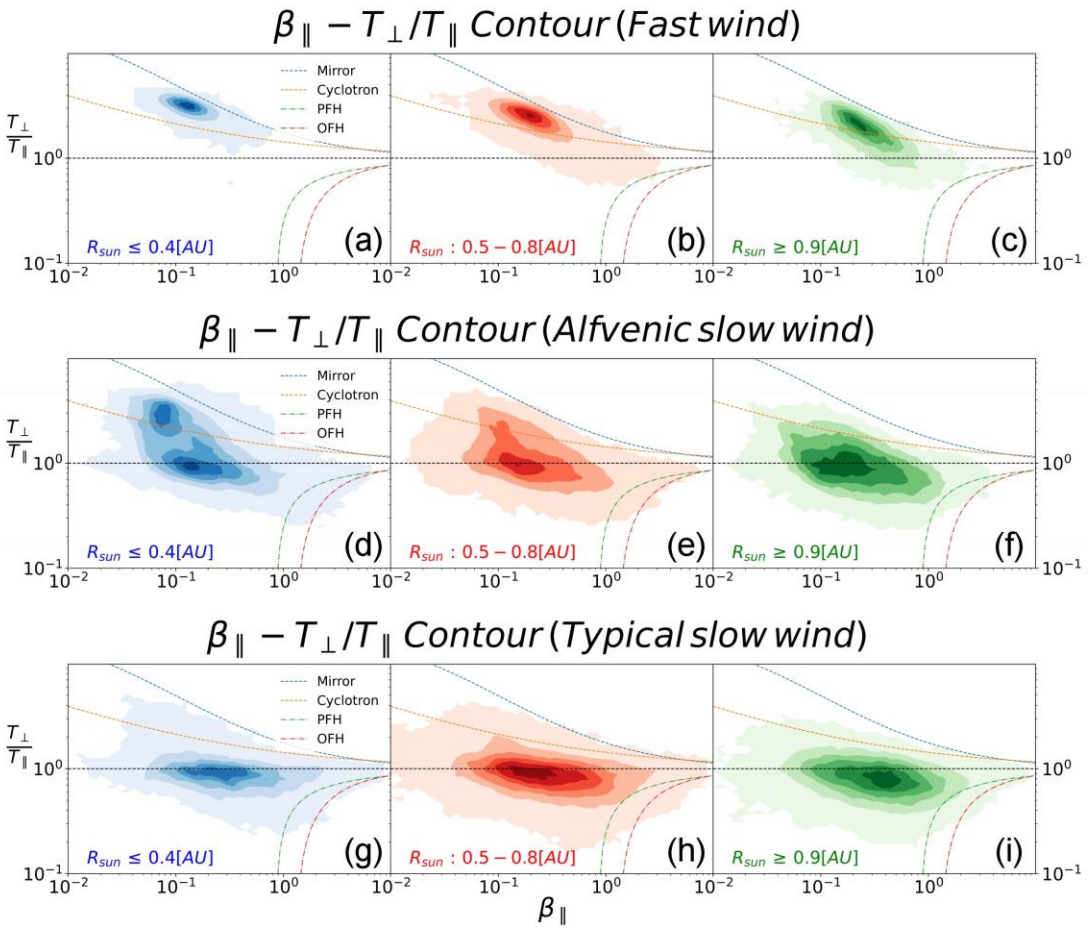

Figure 3. Two-dimensional histogram contours of parallel beta and temperature anisotropy according to distance in three types solar wind. Each indicates below 0.4 au (blue), 0.5-0.8 au (red), and above 0.9 au (green). Color solid or dashed lines are marginal stability conditions for the mirror (blue dashed); ion-cyclotron (orange dashed); parallel (green solid-dashed) and oblique (red solid-dashed) firehose instabilities. Hellinger et al. (2006) gives values of plasma instability condition. The horizon black dashed line denotes isotropic temperature ($\boldsymbol{T}_{\perp}/\boldsymbol{T}_{\parallel} = \mathbf{1}$).

3.2. Detailed investigation of Alfvénic slow wind

We use the Helios-1 data to further investigate the Alfvénic slow wind for three years (1975-1977) during the solar minimum of solar cycle 21. Because the magnetic field structure of the Sun in interplanetary space is relatively stable during a solar minimum, we expect that uncertainty in the statistical analysis will be reduced. Similar to the previous studies (Borovsky & Denton 2010; Borovsky 2016; Perrone et al. 2019), we use the specific entropy, $S_p = T_p/n_p^{2/3}$, to further classify the slow Alfvénic wind. We also use it to identify its source regions on the Sun. The specific entropy seems to correlate well with the heavy ion charge state ratio during a solar minimum: This ratio freezes in the source region of the Sun and travels almost unchanged. Therefore, this method may be used to identify the source of a solar wind stream (Pagel et al. 2004; Stakhiv et al. 2016). Applying the classification method previously used in Perrone et al. (2019), we identify extended periods (≥ 60 minutes) of nearly constant plasma properties, called flat-tops, and define them as a stream. We assume that the solar wind plasma in a stream did not undergo interaction regions such as CIRs or Shocks, and we associate streams of the same specific entropy with the same or similar source region on the Sun (Siscoe & Intriligator 1993; Pagel et al. 2004).

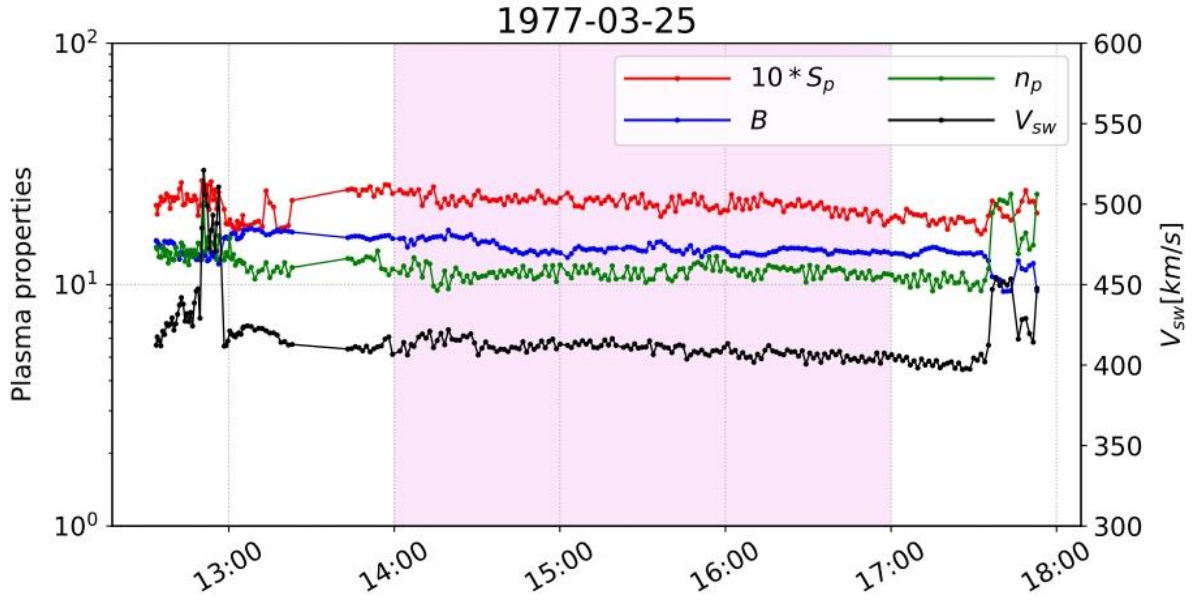

Figure 4. Example of a Alfvénic slow stream observed from Helios-1 on March 25, 1977. Proton specific entropy (red); proton number density (green); magnetic field intensity (blue); and solar wind speed (black). The shaded band is determined to be a Alfvénic slow stream.

In Figure 4, the fluctuations at 13:00 on March 25, 1977 were followed by an extended period (over three hours) of stable plasma parameters. Unlike the high-speed streams ($V_{sw} \geq 600\ km/s$) classified by Perrone et al. (2019) and Hellinger et al. (2011), The Alfvénic slow streams we investigated here have slow solar wind speed ($V_{sw} \leq 450\ km/s$) and tend to last short with a duration of less than a day. It is thought that these Alfvénic slow streams might originate from an equatorial small coronal hole (Bale et al. 2019). Thus, the stream structure and scale are expected to be smaller than those of the high-speed streams that are thought to be generated from the polar coronal holes (D'Amicis & Bruno 2015; Bale et al. 2019; Wang et al. 2019; D'Amicis et al. 2019).

We identify stream events during the solar minimum from 1975 to 1977 and classify them into three groups according to the specific entropy. As shown in Figure 5a, streams A, B, and C are associated with $S_p \geq 2, 0.7 < S_p < 2$, and $S_p \leq 0.7$, respectively. Figure 5b displays histograms of solar wind speed for the three streams. The stream with a larger entropy tends to have a larger solar wind speed, and vice versa. Comparing with the high-speed streams investigated by Perrone et al. (2019), the Alfvénic slow wind streams identified as such are characterized by relatively lower values of specific entropy. This is due to the different plasma conditions, i.e., lower n_p and high T_p, depending on the solar wind speed. Table 1 shows the number of events per year during the survey period.

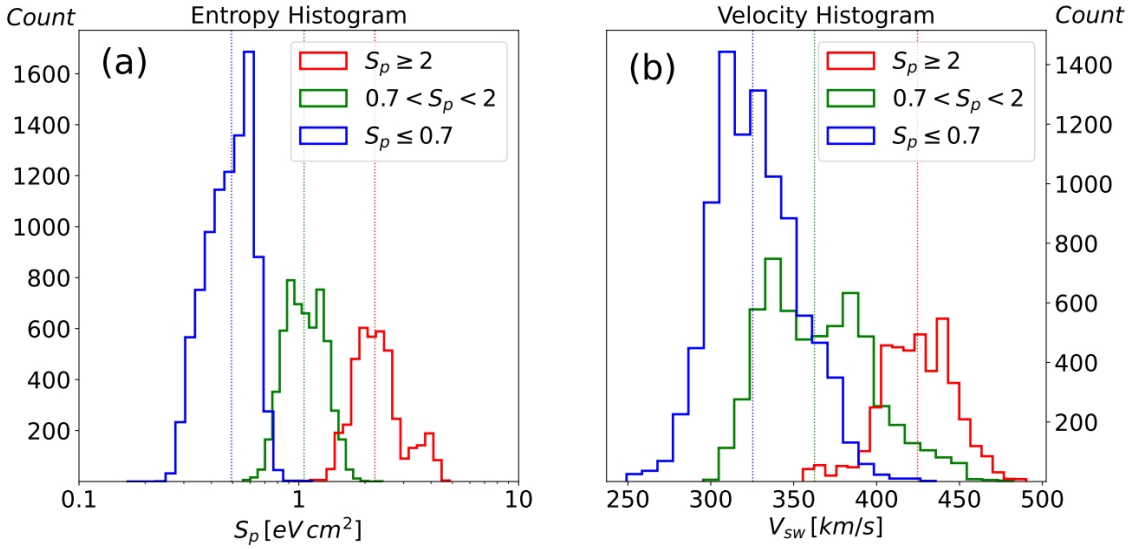

Figure 5. Histograms of (a) the specific entropy and (b) solar wind speed for streams A (red), B (green), and C (blue). The color-coded vertical dotted lines in both panels denote the median values for the corresponding streams. The median values of entropy are 2.22, 1.06, and 0.49 $\boldsymbol{eV\ cm^2}$ for steams A, B, and C, respectively, and the median values of solar wind speed are 425, 363, and 325 $\boldsymbol{km/s}$, respectively.

Table 1

Number of Alfvénic slow streams identified in Helios-1 from 1975 to 1977

Streams	year			Total (Counts)
	1975 (Counts)	1976 (Counts)	1977 (Counts)	
A ($S_p \geq 2$)	13	6	5	24
B ($0.7 < S_p < 2$)	11	12	12	35
C ($S_p \leq 0.7$)	14	17	12	43

Figure 6 shows the radial dependence of proton density, temperature and collisional age in the streams. For all streams, with an increasing radial distance, the temperature and density decrease and the collisional age tends to increase. Our results show that T_p and $T_\perp$ decrease more slowly and $T_\parallel$ decreases faster than the double-adiabatic predictions. For the high-speed streams, Perrone et al. (2019) found the radial dependence of temperatures, $T_p \propto R^{-0.9}$, $T_\perp \propto R^{-1.0}$, and $T_\parallel \propto R^{-0.5}$. In comparison, from Figures 6b-6d, we find that T_p, $T_\perp$, and $T_\parallel$ decrease faster with radial distance. The different radial dependences might be caused by various physical processes such as (i) difference in heating process efficiency by Alfvén-wave turbulence, (ii) Coulomb collisions, (iii) and proton heat flux (Matteini et al. 2012). The statistical features of the Alfvénic slow wind streams are detailed below.

Stream A has relatively higher entropy of $S_p \geq 2$, and is characterized by the fastest speed, the lowest density, and the highest temperature among the streams. According to equation (3), the collisional age is expected to be the lowest and hence Coulomb collisions between solar wind protons will occur relatively weakly. In Figure 6e (red), it can be interpreted that solar wind plasma collides 0.15 times on average while traveling up to 1 au. However, Coulomb collisions occur more frequently than the high-speed streams investigated by Perrone et al. (2019), where fast wind protons collide 0.01 times on average over 1 au.

Stream C has the lowest specific entropy of $S_p \leq 0.7$ and characterized by the slowest speed, the highest density, and the lowest temperature. In Figure 6e (blue), the collisional age is the largest and hence Coulomb collisions occur most frequently among the three streams; it can be seen that solar wind plasma collides 1.62 times on average while traveling up to 1 au. Since the perpendicular and parallel temperatures exhibit radial dependences similar to each other (with the power exponent about -1.2), the solar wind protons seem to maintain almost an isotropic distribution throughout the radial evolution. Although there might be the perpendicular heating associated with Alfvénic fluctuations, this result

suggests that the Coulomb collisions might play a crucial role in controlling the thermodynamic evolution of solar wind protons.

Table 2 summarizes the radial dependencies of n_p, T_p, $T_\perp$, $T_\parallel$, and A_c for all streams. From Stream A to C, the proton density increases, temperature decreases, and the effect of Coulomb collisions increases. Clearly, the lower the specific entropy, the lower the proton temperature, and the more frequent the collisions occur. In particular, Stream C is clearly collision-dominant compared to the other streams. In addition, since Stream A data is the least, overall higher uncertainty is seen, and especially in $T_\parallel$. High $T_\parallel$ uncertainty is also found in high-speed stream, which is thought to be an error caused by the use of core-fit data that fitted a bi-Maxwellian function to the proton core population in the temperature estimation method. In other words, it is assumed to occur because secondary components such as the proton-beam or alpha particles are not considered (Alterman et al. 2018; Finley et al. 2019). Furthermore, Huang et al. (2020) mentioned that in a research using Parker Solar Probe, the perpendicular temperature can directly estimate uncertainty, but the uncertainty estimation of parallel temperature requires additional calculations, implying that it may include contributions from $T_\perp$ uncertainty. Recently, Woodham et al. (2021) discovered that switchbacks observed on Parker Solar Probe can also affect the parallel temperature enhancement of solar wind. For these reasons, it is interpreted that a large error appears in the parallel temperature estimation.

Table 2

Radial dependence of Alfvénic slow streams fit by $f(R) = \alpha(R\ /\ 1\ au)^\gamma$

	Stream A		Stream B		Stream C	
	α	γ	α	γ	α	γ
$n_p(cm^{-3})$	3.72	-2.22±0.21	5.37	-2.08±0.13	9.45	-1.87±0.09
$T_p(10^5K)$	0.63	-1.48±0.19	0.39	-1.37±0.16	0.26	-1.19±0.12
$T_\perp(10^5K)$	0.64	-1.67±0.18	0.35	-1.55±0.17	0.25	-1.18±0.13
$T_\parallel(10^5K)$	0.60	-0.89±0.43	0.46	0.98±0.34	0.29	-1.20±0.22
A_c	0.13	0.97±0.20	0.44	0.99±0.18	1.40	0.83±0.15

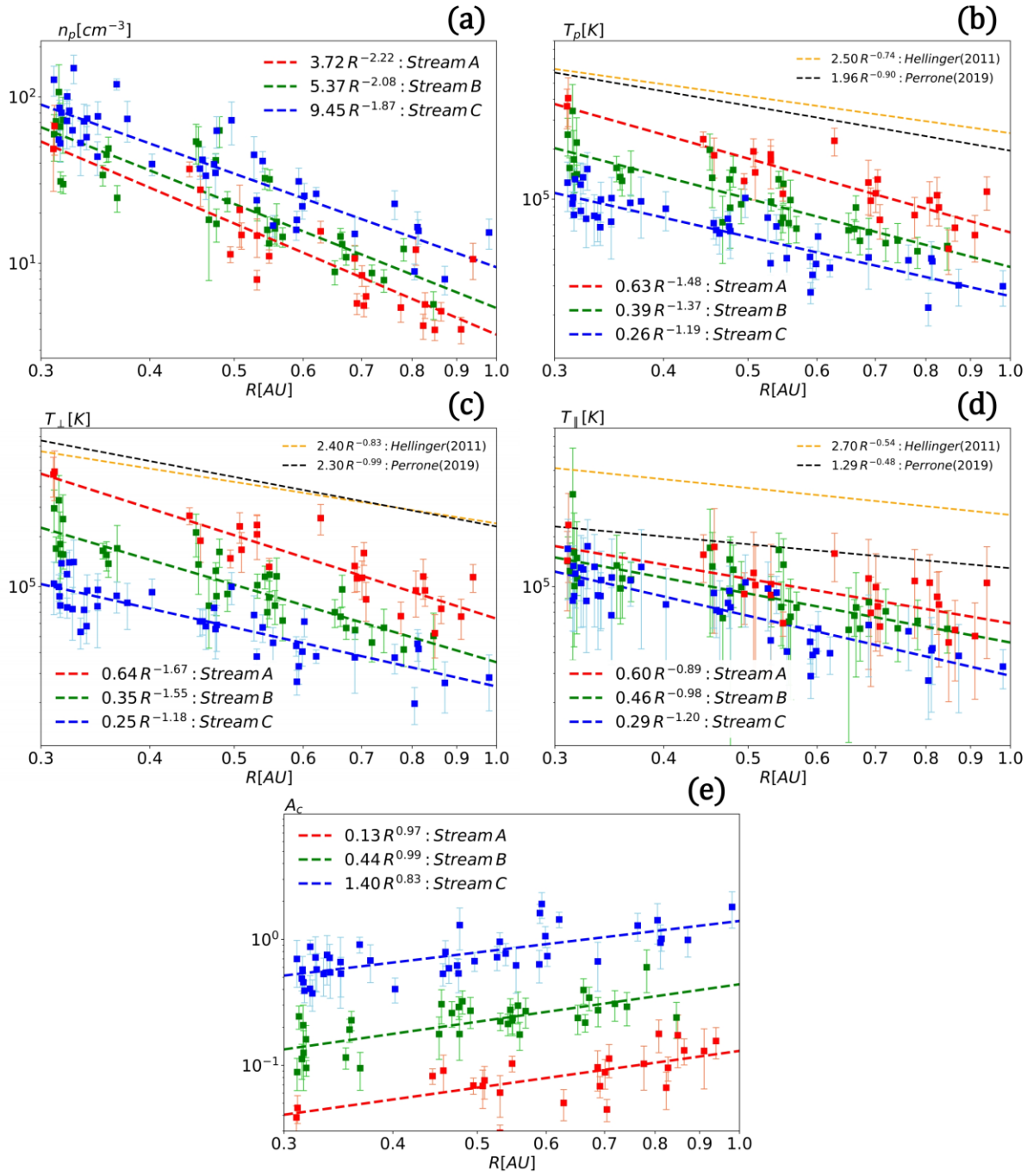

Figure 6. Radial evolution of the three Alfvénic slow streams. (a) $\boldsymbol{n_p}$ (proton density); (b) $\boldsymbol{T_p}$ (proton temperature); (c) $\boldsymbol{T_\perp}$ (perpendicular proton temperature); (d) $\boldsymbol{T_\parallel}$ (parallel proton temperature); (e) $\boldsymbol{A_c}$ (collisional age). Each point and error bar mean the average and standard deviation, and uncertainty is described in more detail in Table 2. Streams A, B, and C are represented by red, green, and blue, respectively. The dashed lines denote the least squares fittings of the relevant parameters for each stream. The temperature dependences investigated by Hellinger et al. (2011) and Perrone et al. (2019) are also shown with the orange and black dotted lines, respectively.

4. Discussion and Conclusion

We have presented a statistical analysis of solar wind protons using the core-fit data of Helios spacecraft and investigated the effect of Coulomb collisions on thermodynamic property. Depending on the solar wind speed and Alfvénicity, we have grouped the solar wind into three-different types and analyzed the collisional property of them, namely, the collisional age. As shown in the previous studies, the fast wind is collision-less and shows a large proton temperature anisotropy, in contrast, the typical slow wind is relatively collision-dominant and exhibits isotropic temperature. The Alfvénic slow wind shows some differences to the typical slow wind in that it tends to have a relatively large proton temperature anisotropy in the collision-less regime and nearly isotropic temperature in the collision-dominant regime.

We have further investigated a detailed analysis of the radial evolution of Alfvénic slow wind during the solar minimum (1975-1977). Based upon the selection method of unperturbed intervals for fast wind streams (Perrone et al. 2019), we have identified the unperturbed plasma characterized by the Alfvénic slow wind. Those slow wind streams are classified into the values of the proton specific entropy.

It is interesting to note that the solar wind stream being a larger entropy appears to be a higher wind speed. It is shown that the overall trend of radial evolution of physical parameters among each Alfvénic slow streams seems to be similar. It is apparent, however, that the values of collisional age are quite different between each streams. Stream A being the highest value of entropy exhibits the lowest number density and highest temperatures, thus resulting in the lowest value of collisional age. As shown in Figure 6, Stream A has an order-of-magnitude lower collisional age than Stream C. These results seem to be quite interesting because even though they are characterized by a similar Alfvénicity, the most important feature among the physical mechanisms responsible for thermodynamic evolution might seem to be different.

It is widely believed that the physical processes regulating the radial evolution of solar wind protons are the double-adiabatic expansion, Coulomb collisions, heating processes, and micro-instabilities (Bale et al. 2009; Matteini et al. 2012; Verscharen et al. 2019). If the Alfvénic fluctuations are considered to be the possible source of perpendicular heating of Alfvénic slow wind protons through some dissipation mechanisms, the perpendicular temperature decreases more slowly with regard to the double-adiabatic prediction. In the case of fast wind streams, it has clearly shown this feature, i.e., the perpendicular temperature anisotropy regardless of the radial distance, shown in the top panel of Figure 3.

Unlike the fast streams, the Coulomb collisions and adiabatic expansion might play a role in controlling the proton temperature anisotropy in the Alfvénic slow streams, even though their effects might differ depending on the plasma environments.

Figure 7 shows a scatter plot of collisional age versus and temperature anisotropy for Alfvénic slow streams classified into three types according to the proton specific entropy. The highlighted colors denote the radial distance from the Sun. As seen in Figure 7a, Stream A near 0.3 au exhibits a large perpendicular temperature anisotropy and low collisional age, indicating that a perpendicular heating process might be dominant over other physical processes. As Stream A expands into the interplanetary

medium and is close to 1 au, the temperature anisotropy might be governed by the adiabatic expansion, and naturally developed kinetic instabilities as well as the heating process (Matteini et al. 2012; Verscharen et al. 2019), thus resulting in the isotropic temperature; the low collisional age near 1 au indicates that the collisional processes have an insignificant influence on the isotropization temperature. However, although Stream C also shows the presence of the Alfvénic fluctuations (possibly, resulting in some heating of protons), it exhibits the near-isotropic (and/or parallel temperature anisotropic) and a relatively large collisional age near 0.3 au shown in Figure 7c. Unlike the case of Stream A, it seems that a perpendicular heating might be weak and/or insignificant. The adiabatic expansion and Coulomb collisions seems to be important processes in regulating the thermodynamic evolution, because they lead to the parallel anisotropy and isotropization of proton temperature, respectively. It is also note that the collisional age gradually increases with the radial distance and becomes greater than the unity near 1 au. This implies that the collisional process is a strong indicator for thermal equilibrium even in the Alfvénic slow streams. This could be identified by comparing the collision timescale with the expansion time.

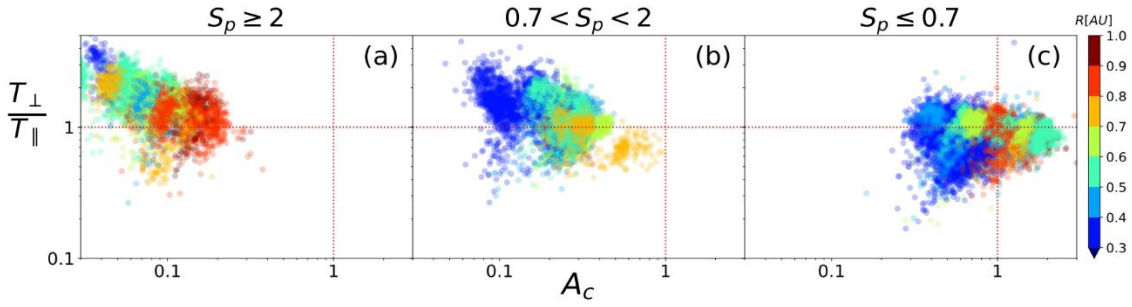

Figure 7. Collisional age, $\boldsymbol{A_c}$, versus temperature anisotropy, $\boldsymbol{T_\perp / T_\parallel}$, scatter plots of Alfvénic slow streams. The distance from the Sun is encoded by the color of the dots. (a) Stream A with higher proton specific entropy; (b) Stream B with intermediate proton specific entropy; (c) Stream C with lower proton specific entropy.

Figure 8 shows a scatter plot of the expansion time versus collision timescale for each stream. Here, the expansion time is defined as $\tau_{exp} = R_0/V_{sw}$, where R_0 and V_{sw} are the distance from the Sun and the solar wind speed, respectively. Also, the collisional timescale is defined to be $\tau_{col} = 1/\nu_{pp}$. Here, the expansion time is calculated using the distance to the observation point (R_{obs}). The black solid line denotes an equal timescale, $\tau_{exp} = \tau_{col}$. For Stream A (red) and B (green), all data are located above the equal timescale, meaning that the collision timescale is much longer than the expansion timescale ($\tau_{col} \gg \tau_{exp}$). Thus it could be thought that for Stream A and B the effect of collisional processes on the radial evolution is weak. For Stream C (blue), on the other hand, these two timescales are comparable. As the τ_{exp} becomes larger (or the radial distance increases), for some portion of Stream C, the collision timescale becomes shorter than the expansion time ($\tau_{col} < \tau_{exp}$), suggesting that the Coulomb collisions could play an important role in regulating the thermodynamic evolution of the Alfvénic slow wind, as the typical slow wind does.

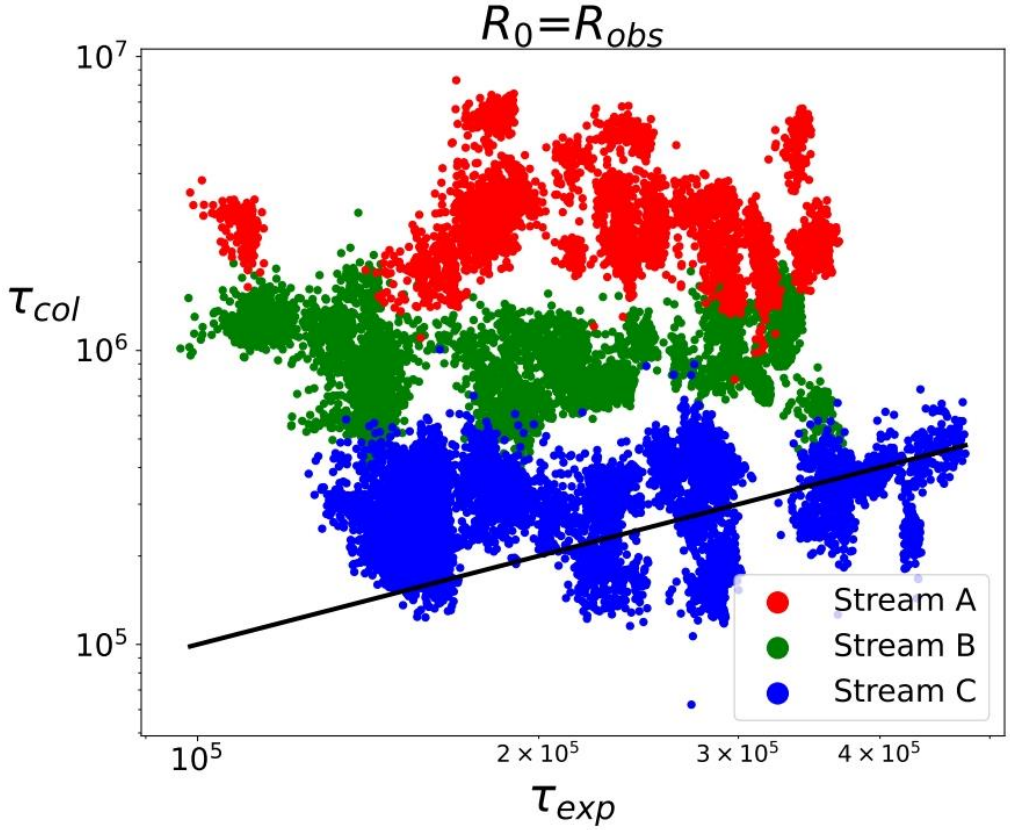

Figure 8. Expansion time ($\boldsymbol{\tau_{exp}}$) versus collision timescale ($\boldsymbol{\tau_{col} = 1/\nu_{pp}}$) for each stream. The black solid line is drawn at $\boldsymbol{\tau_{exp} = \tau_{col}}$. For Streams A (red) and B (green), the effect of Coulomb collisions might be insignificant because the collision timescale is longer than the expansion timescale. For some portion of Stream C (blue), however, these two timescales are comparable, suggesting that collisional process might play a crucial role in the thermodynamic evolution of Alfvénic slow wind.

It has clearly shown that the characteristics of Alfvénic slow streams including the physical mechanisms controlling them could differ from depending upon the proton specific entropy. It might be important to understand where the discrepancy in the specific entropy among the Alfvénic slow streams comes from. This might be closely connected with the solar sources. Previous studies have suggested various sources of Alfvénic slow wind. It is shown that the Alfvénic slow wind might originate from the coronal hole, its boundary, a pseudo-streamers formed at the boundary of extended polar coronal holes, and a small equatorial coronal hole (D'Amicis & Bruno 2015; D'Amicis et al. 2016; Bale et al. 2019; Stansby et al. 2020; D'Amicis et al. 2021). Thus it is expected that among various source regions there is the discrepancy in the proton specific entropy.

Ion composition ratio is generally frozen-in within about five solar radii and travels through interplanetary space with little change (Ko et al. 1999; Von Steiger et al. 2000). For this reason, solar wind plasma shows a difference in ion ratio depending on the source region. For example, fast wind, which is thought to be the source of large polar coronal holes, shows low ion composition ratio, while typical non-Alfvénic

slow wind shows relatively high ion composition ratio (Zurbuchen et al. 2000). Alfvénic slow wind we investigated might be characterized by a low ion composition ratio similar to that of fast wind (D'Amicis et al. 2019). In addition, Pagel et al. (2004) found a well-aligned inverse correlation between oxygen ion charge state ratio and proton specific entropy in the solar activity minimum. Stakhiv et al. (2016) also found the inverse correlation between carbon ion charge state ratio and proton specific entropy. It means that proton specific entropy can act as a reasonably good tracer for the source of solar wind. In our study, we found a difference in entropy of Alfvénic slow wind, which means that even the same type of solar wind can have different source regions depending on the specific entropy.

Stansby et al. (2019) mentioned that Alfvénic and anisotropy solar wind plasma originates from a coronal hole core, and that it generally has high entropy. In contrast, Alfvénic and isotropy solar wind plasma suggests that it originated from the coronal hole edge or active region, and that it has relatively low entropy. In addition, Stansby et al. (2020) suggested that fast wind and Alfvénic slow wind have similar source regions such as coronal holes, but form Alfvénic critical point of different heights depending on the structure of the formed magnetic field. In other words, the properties of solar wind may vary depending on the small difference in the source region or the magnetic field structure at a small scale. Consequently, the entropy may also vary. In our study, the difference between Stream A and C, which are Alfvénic slow wind, is thought to be related to the source region where solar wind plasma was emitted. The coronal hole core is expected to have a relatively smooth open magnetic field without interaction from the surrounding structure. On the other hand, the coronal hole edge is expected to interact with the surrounding magnetic field structure such as pseudo-streamer. So, it is assumed that solar wind in this region has the same property as Stream C (Cranmer 2009; Teriaca et al. 2012). Consequently, the source regions of Alfvénic slow wind suggest the equatorial coronal hole or its boundary structure. Depending on the proton specific entropy, it can be emitted from the coronal hole core or boundary, and Coulomb collision can be affected accordingly.

It will be interesting to map in-situ measurement and magnetic field connectivity with the sun using the PFSS model to find the exact source of Alfvénic slow wind, which will be left as a future exercise. Recently, attempts have been made to discover the source of solar wind through this method (e.g., D'Amicis & Bruno 2015; Wang et al. 2019; Panasenco et al. 2020; D'Amicis et al. 2021). These attempts will enable more accurate tracking of the source region though Parker Solar Probe or Solar Orbiter, which is currently orbiting the sun. In addition, it is also necessary to check whether there is a difference in the source according to the proton specific entropy of Alfvénic slow wind.

5. Acknowledgements

This work was supported by the National Research Foundation of Korea (NRF) Grant funded by the Korea government (MSIT) (2020R1C1C1009996). Data were retrieved using Helios Data Archive[5], Heliopy and processed using pandas. Figures were produced using Matplotlib.

Software: Heliopy (Stansby et al. 2021), Matplotlib (Hunter 2007), Numpy (Harris et al. 2020), pandas (Reback et al. 2021), Scipy (Virtanen et al. 2020), Tslearn (Tavenard et al. 2020).

6. References

Abbo, L., Ofman, L., Antiochos, S.K., et al. 2016, Space Sci. Rev. 201, 22-108

Alterman, B. L., Kasper, J. C., Stevens, M. L., & Koval, A. 2018, ApJ, 864, 112

Bale, S. D., Kasper, J. C., Howes, G. G., et al. 2009, PhRvL, 103, 211101

Bale, S. D., Badman, S. T., Bonnell, J. W., et al. 2019, Natur, 576, 237

Barnes, A. 1968, ApJ, 154, 751

Boldyrev, S., Forest, C., & Egedal, J. 2020, PNAS, 117, 9232

Borovsky, J. E., & Denton, M. H. 2010, JGRA, 115, A10101

Borovsky, J. E. 2016, JGRA, 121, 5055

Bruno, R., & Carbone, V. 2013, LRSP, 10, 2

Chandran, B. D. G., Li, B., Rogers, B. N., Quataert, E., & Germaschewski, K. 2010, ApJ, 720, 503

Chandran, B. D. G., et al. 2011, ApJ, 743, 179

Chen, W., Lai, S., Liu, H., & Lin, W. 1972, JGR, 77, 1

Chew, G. F., Goldberger, M. L., & Low, F. E. 1956, RSPSA, 236, 112

Chhiber, R., Usmanov, A., Matthaeus, W., & Goldstein, M. 2016, ApJ, 821, 34

Cranmer, S. R. 2009, LRSP, 6, 3

Cuturi, M., & Blondel, M. 2017, PMLR, 70, 894

D'Amicis, R., & Bruno, R. 2015, ApJ, 805, 84

D'Amicis, R., Bruno, R., & Matteini, L. 2016, in AIP Conf. Proc. 1720, 040002

D'Amicis, R., Matteini, L., & Bruno, R. 2019, MNRAS, 483, 4665

D'Amicis, R., Perrone, D., Bruno, R., & Velli, M. 2021, JGRA, 126, e28996

D'Amicis, R., Bruno, R., Panasenco, O., et al. 2021, A&A, 656, A21

Dougal, A. A., & Goldstein, L. 1958, Phys. Rev., 109, 615

Finley, A. J., McManus, M. D., Matt, S. P., et al. 2021, A&A, 650, A17

Fox, N. J., Velli, M. C., Bale, S. D., et al. 2016, SSRv, 204, 7

Harris, C. R., Millman, K. J., van der Walt, S. J., et al. 2020, Natur, 585, 357

Hellinger, P., Trávníček, P. M., Kasper, J. C., & Lazarus, A. J. 2006, GeoRL, 33, L09101

Hellinger, P., Matteini, L., Štverák, Š., Trávníček, P. M., & Marsch, E. 2011, JGRA, 116, A09105

Hellinger, P., & Trávníček, P. M. 2014, ApJL, 784, L15

[5] https://helios-data.ssl.berkeley.edu/

Huang, J., Kasper, J. C., Vech, D., et al. 2020, ApJS, 246, 70
Hunter, J. D. 2007, CSE, 9, 90
Kasper, J. C., Lazarus, A. J., & Gary, S. P. 2008, PhRvL, 101, 261103
Kasper, J. C., Klein, K. G., Weber, T., et al. 2017, ApJ, 849, 126
Klein, L. W., Ogilvie, K. W., & Burlaga, L. F. 1985, JGRA, 90, 7389
Ko, Y.-K., Gloeckler, G., Cohen, C. M. S., & Galvin, A. B. 1999, JGR, 104, 17005
Livi, S., Marsch, E., & Rosenbauer, H. 1986, JGR, 91, 8045
Marsch, E., & Goldstein, H. 1983, JGRA, 88, 9933
Martinovic M. M., Klein K. G., Bourouaine S., 2019, ApJ, 879, 43
Matteini, L., Landi, S., Hellinger, P., et al. 2007, GeoRL, 34, 20105
Matteini, L., Hellinger, P., Landi, S., et al. 2012, Space Sci. Rev., 173, 373-396
Meyer-Vernet, N. 2007, Basics of the Solar Wind (Cambridge: Cambridge Univ. Press)
Pagel, A. C., Crooker, N. U., Zurbuchen, T. H., & Gosling, J. T. 2004, JGR,109, A01113
Panasenco, O., Velli, M., D'Amicis, R., et al. 2020, ApJS, 246, 54
Perez, J. C., Chandran, B. D. G., Klein, K. G., & Martinović, M. M. 2021, JPP, 87, 905870218
Perrone, D., Stansby, D., Horbury, T. S., & Matteini, L. 2019, MNRAS, 483, 3730
Perrone, D., D'Amicis, R., De Marco, R., et al. 2020, A&A, 633, A166
Porsche, H. 1977, JGR, 42, 551
Reback, J., jbrockmendel, Mckinney, W., et al. 2021, pandas-dev/pandas: Pandas 1.3.4, Zenodo
Sakoe, H., & Chiba, S. 1978, ITASS, 26, 43
Salem, C., Hubert, D., Lacombe, C., et al. 2003, ApJ, 585, 1147
Schunk, R. W. 1975, P&SS, 23, 437
Siscoe, G. L., & Intriligator, D. 1993, GeoRL, 20, 2267
Stakhiv, M., Lepri, S. T., Landi, E., Tracy, P., & Zurbuchen, T. H. 2016, ApJ, 829, 117
Stansby, D., Salem, C., Matteini, L., & Horbury, T. 2018, SoPh, 293, 155
Stansby, D., Horbury, T. S., & Matteini, L. 2019, MNRAS, 482, 1706
Stansby, D. 2019, The solar wind in the inner heliosphere
Stansby, D., Matteini, L., & Horbury, T. S. 2020, MNRAS, 492, 39
Stansby, D., Rai, Y., Argall, M., et al. 2021, heliopython/heliopy: HelioPy 0.15.4, Zenodo
Štverák, S., Trávníček, P., Maksimovic, M., et al. 2008, JGRA, 113, 3103
Tavenard, R., Faouzi, J., Vandewiele, G., et al. 2020, JMLR, 21, 118
Teriaca, L., Andretta, V., Auchère, F., et al. 2012, ExA, 34, 273
van Ballegooijen, A. A., & Asgari-Targhi, M. 2016, ApJ, 821, 106
Verscharen, D., Klein, K. G., & Maruca, B. A. 2019, LRSP, 16, 5
Virtanen, P., Gommers, R., Oliphant, T. E., et al. 2020, Nat. Methods, 17, 261
von Steiger, R., Schwadron, N. A., Fisk, L. A., et al. 2000, JGR, 105, 27217
Wang, X., Zhao, L., Tu, C., & He, J. 2019, ApJ, 871, 204

Wang, Y.-M., & Ko, Y.-K. 2019, ApJ, 880, 146
Wilson, L. B., III, Stevens, M. L., Kasper, J. C., et al. 2018, ApJS, 236, 41
Woodham, L. D., Horbury, T. S., Matteini, L., et al. 2021, A&A, 650, L1
Yoon, P. H., Seough, J., Salem, C. S., & Klein, K. G. 2019, PhRvL, 123, 145101
Zurbuchen, T. H., Hefti, S., Fisk, L. A., Gloeckler, G., & Schwadron, N. A. 2000, JGR, 105, 18327